



Article

The Effect of Different Amounts of Conductive Carbon Material on the Electrochemical Performance of the LiFePO₄ Cathode in Li-Ion Batteries

Debabrata Mohanty ¹, Min-Jie Chang ¹ and I-Ming Hung ^{1,2,*}¹ Department of Chemical Engineering and Materials Science, Yuan Ze University, 135 Yuan-Tung Road, Chung-Li, Taoyuan 32003, Taiwan; debabrata.mohanty@cgcu.edu.tw (D.M.); tracy881017@gmail.com (M.-J.C.)² Hierarchical Green-Energy Materials (Hi-GEM) Research Center, National Cheng Kung University, Tainan 70101, Taiwan

* Correspondence: imhung@saturn.yzu.edu.tw; Tel.: +886-3-463-8800

Abstract: LiFePO₄ (LFP) has undergone extensive research and is a promising cathode material for Li-ion batteries. The high interest is due to its low raw material cost, good electrochemical stability, and high-capacity retention. However, poor electronic conductivity and a low Li⁺ diffusion rate decrease its electrochemical reactivity, especially at fast charge/discharge rates. In this work, the volumetric energy density of lithium-ion batteries is successfully increased by using different amounts of conductive carbon (Super P) in the active material content. The particle size and morphology of the electrode material samples are studied using field emission scanning electron microscopy and dynamic light scattering. Two-point-probe DC measurements and adhesive force tests are used to determine the conductivity and evaluate adhesion for the positive electrode. Cyclic voltammetry, electrochemical impedance spectroscopy (EIS), and charge/discharge tests are used to analyze the electrochemical properties of the battery. The samples containing 88% LFP, 5.5% Super P, and 6.5% PVDF perform best, with discharge capacities reaching 169.8 mAh g⁻¹ at 0.1 C, and they can also manage charging/discharging of 5 C. EIS indicates that this combination produces the lowest charge-transfer impedance (67 Ω) and the highest Li⁺ ion diffusion coefficient (5.76×10^{-14} cm² s⁻¹).



Citation: Mohanty, D.; Chang, M.-J.; Hung, I.-M. The Effect of Different Amounts of Conductive Carbon Material on the Electrochemical Performance of the LiFePO₄ Cathode in Li-Ion Batteries. *Batteries* **2023**, *9*, 515. <https://doi.org/10.3390/batteries9100515>

Academic Editor: Argyrios Karatrantos

Received: 19 September 2023

Revised: 13 October 2023

Accepted: 18 October 2023

Published: 20 October 2023



Copyright: © 2023 by the authors. Licensee MDPI, Basel, Switzerland. This article is an open access article distributed under the terms and conditions of the Creative Commons Attribution (CC BY) license (<https://creativecommons.org/licenses/by/4.0/>).

1. Introduction

In-depth research has recently focused on the large-scale application of Li-ion batteries in hybrid electric vehicles (HEVs) and backup power systems. Although LiCoO₂ is already successfully commercialized in small lithium-ion batteries, using it as the cathode material in large-scale lithium-ion batteries is still challenging due to safety problems and high cost [1,2]. Due to its relatively low cost and safer operation, LiFePO₄ is considered an ideal material to utilize as the cathode in large-scale lithium-ion batteries [3,4]. The additional benefits of LiFePO₄-based batteries for powering electric vehicles (EVs) and plug-in hybrid electric vehicles (PHEVs) are their high theoretical capacity (170 mAh g⁻¹), good electrochemical window (2–4 V), superior cycle performance, excellent thermal stability, environmental friendliness, low self-discharge, and the safety of olivine-type LiFePO₄ [5–8]. For two decades, LiFePO₄ has been the subject of extensive research for both scientific and engineering applications [9]. Despite the numerous benefits, LiFePO₄ in LIBs still faces challenges, particularly because of the suboptimal low-temperature electrochemical performance in its transportation applications [10,11]. The low electrical conductivity of LiFePO₄ (around 10^{-9} to 10^{-10} S cm⁻¹ at room temperature) and its slow lithium-ion diffusivity (around 10^{-14} to 10^{-16} cm² s⁻¹ at room temperature) are the main reasons for its relatively poor low-temperature electrochemical performance [12]. This is contrary to

earlier reports that claim that the choice of the cathode material largely determines the low-temperature electrochemical performance of the battery [13]. It is being highlighted that electrolytes, as well as electrodes, play a role in the low-temperature performance of LIBs. Since electrolytes not only function as a Li-ion running phase but additionally take on a role in electrolyte-interface reactions, like the development of solid electrolyte interfaces (SEI) and electrode reactions, substantial attempts have been made over the past ten years to enhance the low-temperature conductivity of electrolytes [14]. It is clear that inadequate performance at low temperatures is directly correlated with the decreased ionic conductivity of electrolytes and the SEI. Nevertheless, a slow electrode reaction caused by the electrolyte part is related to the electrolyte-interface properties, including the wettability of the electrode and the composition of solvated Li-ion, in addition to ionic conductivity [15]. Ionic conductivity affects the rate of charge and decreases in discharge, leading to reduced battery capacity and power output. Low temperatures can cause the electrolyte to become more viscous [16]. The low-temperature environment can significantly slow down the diffusion of ions as well as impact the safety of the battery [17]. Addressing these limitations often involves designing or selecting a battery system that can maintain its performance at low temperatures. Additionally, improving the overall thermal management of the battery can help mitigate the impact of low temperatures on performance.

Shin et al. discovered, in 2013, that pure LiFePO₄ improves battery cycle stability at lower operating temperatures (20 °C) [18]. It was also found that bulk- and surface-deterioration was significantly reduced for low temperatures. In addition, significant efforts were made to improve the low-temperature electrochemical performance of the LiFePO₄ cathode, which include the following: (i) coating the surface of LiFePO₄ with carbon or other conducting materials to increase the electronic conductivity [19], (ii) reducing the particle size to shorten diffusion distances and increase the surface area [20], and (iii) doping with super-valent cations or metal oxides to improve the intrinsic electronic conductivity [21]. Moreover, both the surface reaction kinetics and the rate of charge (for lithium-ions and electrons) diffusion inside the electrode bulk slow down with decreasing operating temperature [22,23]. Consequently, the electrode faces a greater challenge under such conditions.

Generally, carbon coating is considered highly efficient as it hinders particle growth during sintering, leading to reduced particle size. Additionally, it enhances the electronic conductivity of the active particles' surface [24–26]. This method is widely used and extensively studied. In other words, the combination of smaller particle size and carbon coating should significantly enhance the electrochemical performance of LiFePO₄ [27]. In LFP (LiFePO₄)-based cathodes, various conductive fillers have been investigated, revealing a wide range of materials and techniques aimed at improving the electrochemical performance of these energy storage systems [28]. These are alternative fillers, whereas conventional carbon additives, such as carbon black and graphite, have historically been crucial in improving electronic conductivity within LFP cathodes [29]. Due to their exceptional electrical conductivity and mechanical toughness, carbon nanotubes (CNTs) have emerged as a promising candidate [30]. Additionally, conductive polymer coatings have drawn attention for their potential to improve electronic and ionic conductivity while minimizing problems with carbon agglomeration. These coatings can be used alone or in conjunction with conventional carbon materials. LiFePO₄ materials with carbon coatings were successfully created by Zhao et al. in 2016, using polystyrene spheres (50–300 nm) as the carbon source [31]. The results showed that LiFePO₄/C, which contains 3.0 percent carbon weight, performed well electrochemically at 20 °C, delivering 147 mAh g⁻¹ and 79.3 mAh g⁻¹ at 0.1 C and 1 C. Moreover, LiFePO₄/C showed approximately 100% capacity retention—even after 100 cycles at 1 C. This is due to the ideal thickness (2.5 nm) and suitable shape of the carbon coating [32]. As an alternative, Yang et al. studied LiFePO₄/C porous microspheres with a double carbon coating and found an outstanding specific discharge capacity of 120 mAh g⁻¹ (10 C) at 20 °C [33]. Additionally, utilizing polyvinylpyrrolidone and citric acid as complex carbon sources, Liu et al. examined LiFePO₄/C nanoparticles with a

diameter of roughly 80 nm [34]. Due to their small size and uniformly thin carbon coating, these nanoparticles demonstrated a good discharge capacity (126 mAh g^{-1}) at a discharge rate of 0.1 C at 20 °C.

In addition to conductive carbon coatings, metal ion doping is often used to increase LiFePO₄ conductivity [35]. In order to effectively increase the low-temperature and high-rate performance of LiFePO₄, Zhang et al. combined carbon aerogel coating and metal-ion doping (lanthanum- and cerium-doped LiFePO₄/C) [36]. Co-precipitation was used by Yang et al. to create a LiMn_{0.8}Fe_{0.2}PO₄/C cathode. In this way, both improved rates and low-temperature capabilities could be obtained [37]. Nano-LiMn_{0.8}Fe_{0.2}PO₄/C supplied 97 mAh g⁻¹ at 0.1 C—even at low temperatures (15 °C). LiFePO₄/C-Sn exhibited excellent electrochemical performance across a wide range of operating temperatures, particularly at low temperatures, when Lin et al. coated the surface of LiFePO₄ with Sn nanoparticles [38]. It appears that all prior studies of the low-temperature performance of LiFePO₄ consistently showed that its reversible capacity and rate capability could be significantly reduced during operation at low temperatures [39].

Increasing the driving range and enhancing lithium-ion battery longevity are the two primary development goals for electric cars. The energy density of lithium-ion batteries directly affects their longevity, and their endurance increases with increasing energy density, as well as extending the operational temperature range and reducing charging time. In addition, enhancing the energy density of lithium-ion batteries can be achieved in several ways [40]. The injection volume of the entire battery can be reduced by increasing the difference between the median voltages of the positive and negative electrode, as well as the gram capacity of the positive and negative electrode [41,42]. If the positive electrode materials are of identical types and the lithium-ion battery's overall weight and positive electrode volume are fixed, the energy density can be increased by increasing the positive electrode material's proportion rather than its overall volume [43]. Furthermore, reduced capacitance during fast charge and discharge can be due to very high resistance, inadequate adhesion, and a decreased ratio of conductive carbon to binder [44]. Presently, cathode materials constitute 70% of the materials used in academic research. Thus, the percentage of LFP was increased in this study to 88%, and the electrochemical performance and mechanical stability were taken into account using the best active carbon–material balance ratio.

2. Results and Discussion

FE-SEM images of Super P conductive carbon at different magnifications are shown in Figure 1a–d. Super P appears granular, and stacking occurs. This characteristic of Super P can facilitate the filling of the positive electrode material's particles. To develop positive LFP electrode materials with the optimal amount of conductive additive and binder, the LiFePO₄ mother powder was supplemented with varying quantities of Super P conductive carbon material as an additive.

The adhesion force measurement was carried out with an adhesion tester (MIT-AT12). To obtain samples for the adhesion test, we cut 100 tiny squares ($0.25 \times 0.25 \text{ cm}^2$) into the surface of a positive LiFePO₄ electrode sheet made with different Super P ratios. The cutting speeds were 20 to 50 mm/s in the horizontal and vertical directions. To evaluate the adherence of the LiFePO₄ cathode coating, any burrs were removed with a soft brush, and the sample was attached to the grid's surface with a special test tape. The peeling of the surface coat was evaluated according to six different categories—see Table 1. Figure 2a–f show the adhesion test results of the SP_3%, SP_4%, SP_5%, SP_5.5%, SP_6%, and SP_7% samples. The SP_3% sample showed the strongest adhesion, with only small pieces peeling off at the incision's intersection. On the other hand, the SP_7% sample showed large pieces that peeled off at the edges of the squares, which suggests the weakest adhesion. The adhesion steadily declines as the amount of conductive carbon material increases (and the amount of binder decreases). Table 2 shows the adhesion grade for all samples. AC impedance analysis is one of the most complex techniques

in electrochemical research. It is an AC test technique where a sine wave signal with a specific amplitude, but variable frequency, is applied to the electrochemical system to receive current feedback. The charge transfer resistances and Li^+ ion diffusion coefficients of LiFePO_4 cathode material samples were determined using a coin cell battery configured as a “prepared LiFePO_4 cathode//lithium hexafluorophosphate LiPF_6 + ethylene carbonate (EC)/dimethyl carbonate (DMC)+ vinylene carbonate (VC) electrolyte//Li metal” in the frequency range of 7×10^6 —0.01 Hz under open circuit voltage.

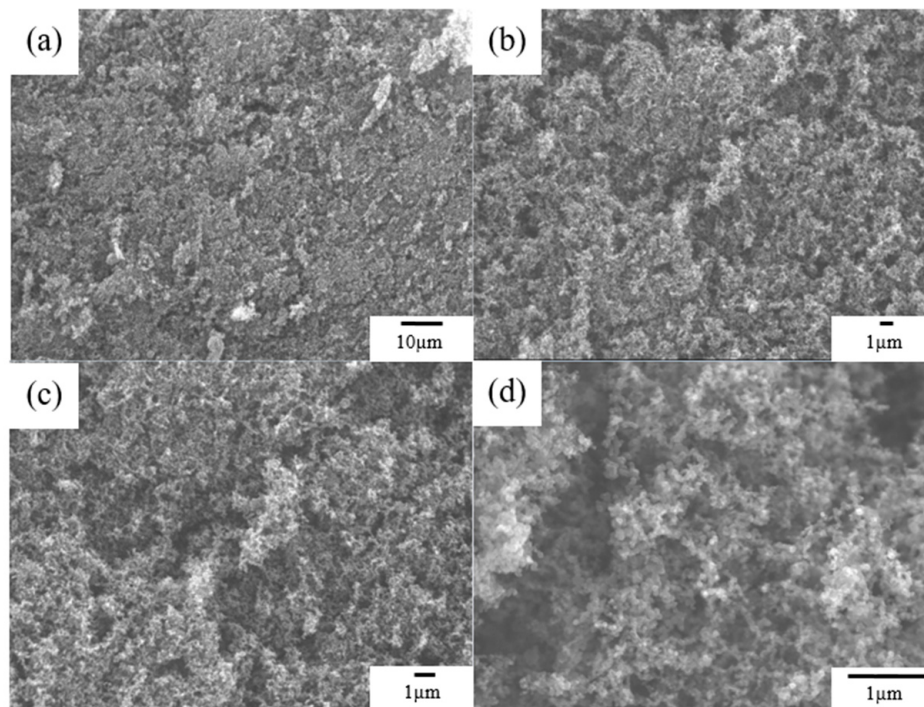


Figure 1. FE-SEM micrograph of Super P at different magnifications of (a) $\times 1000$, (b) $\times 3000$, (c) $\times 5000$, and (d) $\times 20,000$.

Table 1. Adhesion test standards.

ISO Level	ASTM Grade	Test Results
0	5B	The edge of the incision is completely smooth, and the edge of the grid has not peeled off.
1	4B	There are small pieces peeling off at the intersection of the cuts, and the actual damage in the scribed area does not exceed 5%.
2	3B	The edges and/or intersections of the incisions have peeled off, with an area of more than 5%, but less than 15%.
3	2B	Partially chipped or completely chipped along the edge of the notch, and the partially chipped was stripped by more than 15%, but less than 35%.
4	1B	The edge of the cut is flaking or/and partly squared or partially peeled off, and the area is larger than the 35% mark of the grid area, but not more than 65%.
5	0B	Beyond the previous level.

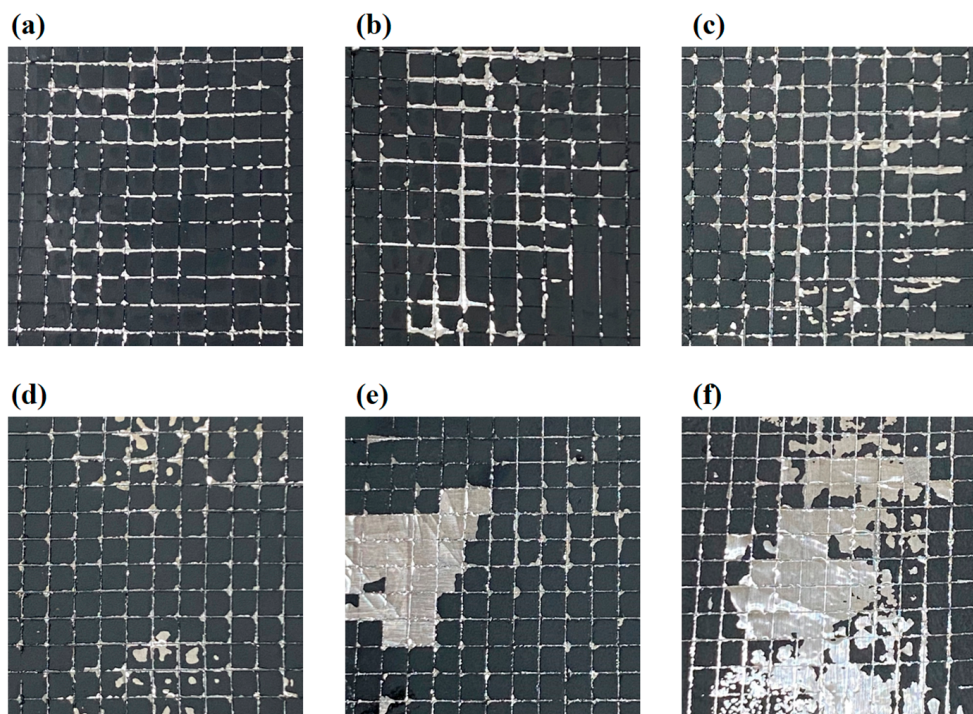


Figure 2. Adhesive force measurement of (a) SP_3%, (b) SP_4%, (c) SP_5%, (d) SP_5.5%, (e) SP_6%, and (f) SP_7% samples.

Table 2. Adhesion test result rating for SP_3%, SP_4%, SP_5%, SP_5.5%, SP_6%, and SP_7% samples.

Sample	ISO Level	ASTM Grade
SP_3%	1	4B
SP_4%	2	3B
SP_5%	2	3B
SP_5.5%	2	3B
SP_6%	4	1B
SP_7%	5	0B

The curve features two distinct segments: a high-frequency semicircle and a low-frequency oblique straight line. These represent the charge-transfer process and the diffusion resistance of the Li^+ ion in the electrochemical reaction, respectively, when the electrode reaction is controlled by both charge transfer and Li^+ ion diffusion [45]. Here the Randles equivalent circuit [46] was used as a fitting model, and EIS was used to simulate the Li^+ diffusion process. R_e denotes the combined resistance of the electrolyte and electrode material, also known as the solution resistance. This value is indicated by the high-frequency region's semicircle intercept. The charge transfer resistance of the positive electrode/electrolyte interface, represented by R_{ct} , is the diameter of the semicircle. Z_w is the reaction-diffusion process's Warburg impedance, which corresponds to the oblique line in the low-frequency region, from which the Li^+ ion diffusion coefficient can be calculated. The resulting AC impedance curves are shown in Figure 3. It can also be plotted as a function of $\omega^{-1/2}$ (ω is the angular frequency, $\omega = 2\pi f$) using the real impedance (Z'), which is shown in Figure 4. The slope σ (Equation (1)) [47] is obtained from the linear fit of Z' to $\omega^{-1/2}$ from Figure 4, and the value of the slope is substituted in Equation (2) [48] to calculate the Li^+ ion diffusion coefficient (D_{EIS}) of the battery.

$$Z' = R_e + R_{ct} + \sigma \omega^{-1/2} \quad (1)$$

$$D_{EIS} = R^2 T^2 / 2 A^2 n^4 F^4 C^2 \sigma^2 \quad (2)$$

where R: gas constant ($\text{J K}^{-1} \text{ mol}^{-1}$), T: working temperature (K), A: pole piece area (cm^2), n: number of electrons transferred, F: Faraday's constant (C mol^{-1}), and C: concentration of lithium ions in the cathode material (mole cm^{-3}).

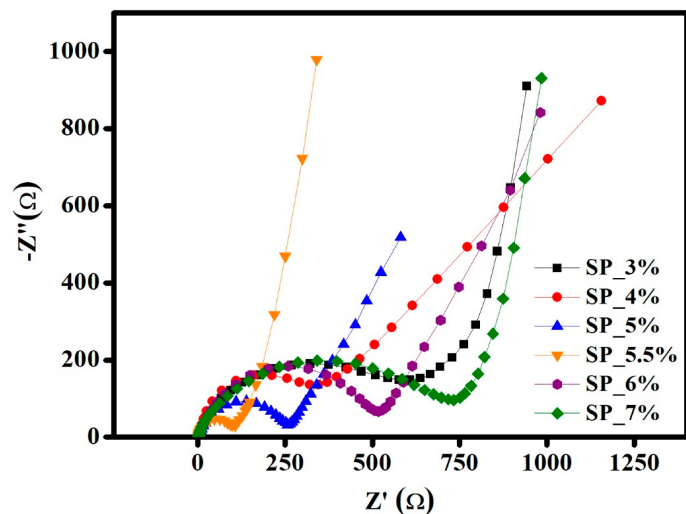


Figure 3. AC impedance spectra of SP_3%, SP_4%, SP_5%, SP_5.5%, SP_6%, and SP_7% samples at OCV.

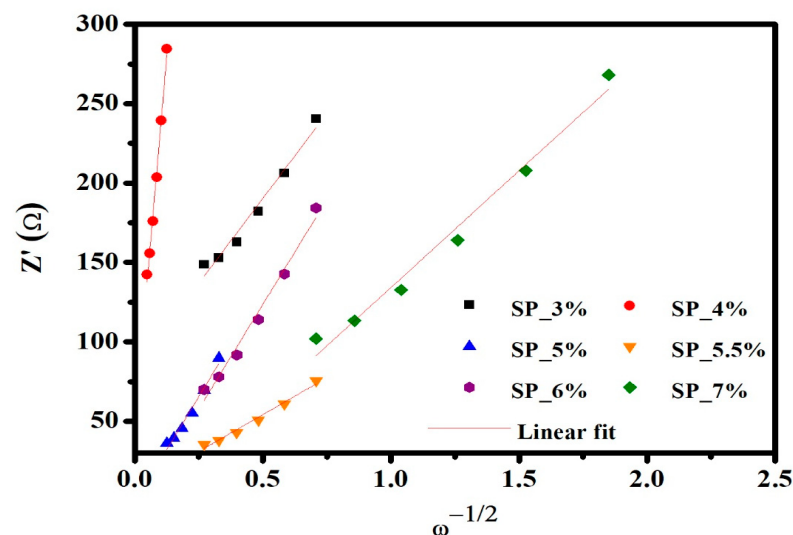


Figure 4. The relationship between Z' and $\omega^{-1/2}$ at low frequencies of SP_3%, SP_4%, SP_5%, SP_5.5%, SP_6%, and SP_7% samples at OCV.

Table 3 shows the results of the impedance simulation and the resulting Li^+ ion diffusion coefficient. Based on these findings, SP_5.5% has the lowest charge-transfer resistance (67Ω) and the highest Li^+ ion diffusion coefficient, whereas SP_4% has the highest electrode resistance (9.97Ω) and the lowest Li^+ ion diffusion coefficient. SP_5.5% has a lower Re than all other samples, and the sample battery has a higher Re before the discharge test. This suggests that the diffusion resistance of Li^+ ions between solutions is higher. Additionally, it has been shown that the sample's charge-transfer resistance first increases before it decreases as the amount of conductive carbon increases. The trend remains unchanged despite an order of magnitude divergence from the Li^+ ion diffusion coefficient determined based on CV. Hence, the ideal fractions for LiFePO_4 , Super P, and PVDF are $\text{LiFePO}_4 = 88\%$, Super P = 5.5%, and PVDF = 6.5%.

Table 3. The impedance parameters of SP_3%, SP_4%, SP_5%, SP_5.5%, SP_6%, and SP_7% samples at OCV.

Sample	R_e (Ω)	R_{ct} (Ω)	D_{EIS} ($\text{cm}^2 \text{ s}^{-1}$)
SP_3%	2.33	338	1.08×10^{-14}
SP_4%	9.97	284	1.45×10^{-16}
SP_5%	2.71	199	6.99×10^{-15}
SP_5.5%	1.87	67	5.76×10^{-14}
SP_6%	2.26	372	7.13×10^{-15}
SP_7%	2.13	412	2.89×10^{-14}

The redox behavior of materials throughout the charging/discharging process was examined using cyclic voltammetry. To determine the relationship between voltage and current, testing involved fixing the scan cut-off voltage range, setting a certain scan rate, and repeated scanning. Here, six different scan rates ($0.1, 0.2, 0.25, 0.5, 0.75$, and 1 mV s^{-1}) were chosen, with the cut-off voltage varying from 2.8 to 4.0 V. The oxidation of the samples can be seen in Figure 5. The figure shows the CV curves for the SP_3%, SP_4%, SP_5%, SP_5.5%, SP_6%, and SP_7% samples and a scan rate of 0.1 mV s^{-1} . The most symmetrical and sharply decreasing peak indicates the highest electrochemical reversibility as well as the easiest intercalation and deintercalation of Li^+ ions for the given ratio. The redox findings of the samples SP_3%, SP_4%, SP_5%, SP_5.5%, SP_6%, and SP_7% at various scan rates are shown in Figure 6a–f. Furthermore, the peak currents associated with the oxidation and reduction peaks increase with the scan rate. The voltage difference (ΔV) between the redox peaks also widens gradually, which reflects the polarization of the positive electrode. It also increases and changes to a higher potential and lower potentials, respectively. The smaller the ΔV is, the less pronounced the polarization is. Table 4 shows the ΔV values for every sample at different scan speeds. SP_5.5% has the smallest ΔV (representing the intercalation/deintercalation of Li^+ ions into LFP) among all scan rates—as well as excellent reversibility. In addition, SP_5.5% also shows the lowest polarization, the best kinetic performance, and the best electrochemical reversibility.

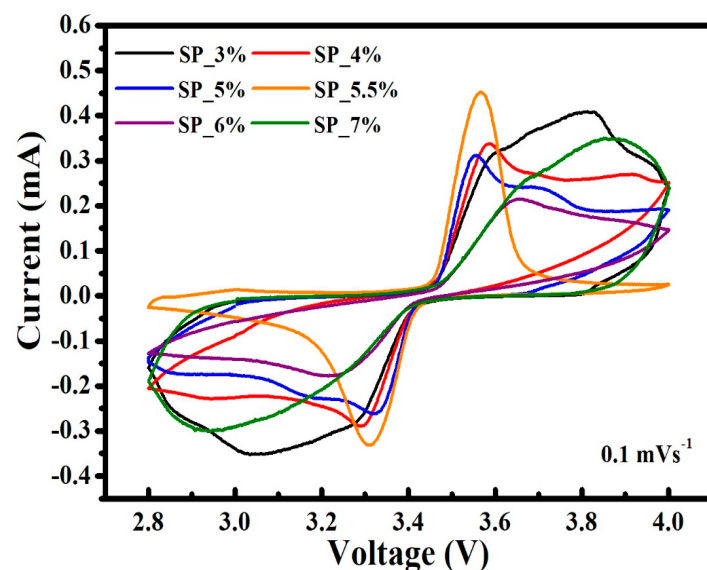


Figure 5. Cyclic voltammetry profiles of SP_3%, SP_4%, SP_5%, SP_5.5%, SP_6%, and SP_7% samples with scanning rate of 0.1 mVs^{-1} between 2.8 and 4.0 V.

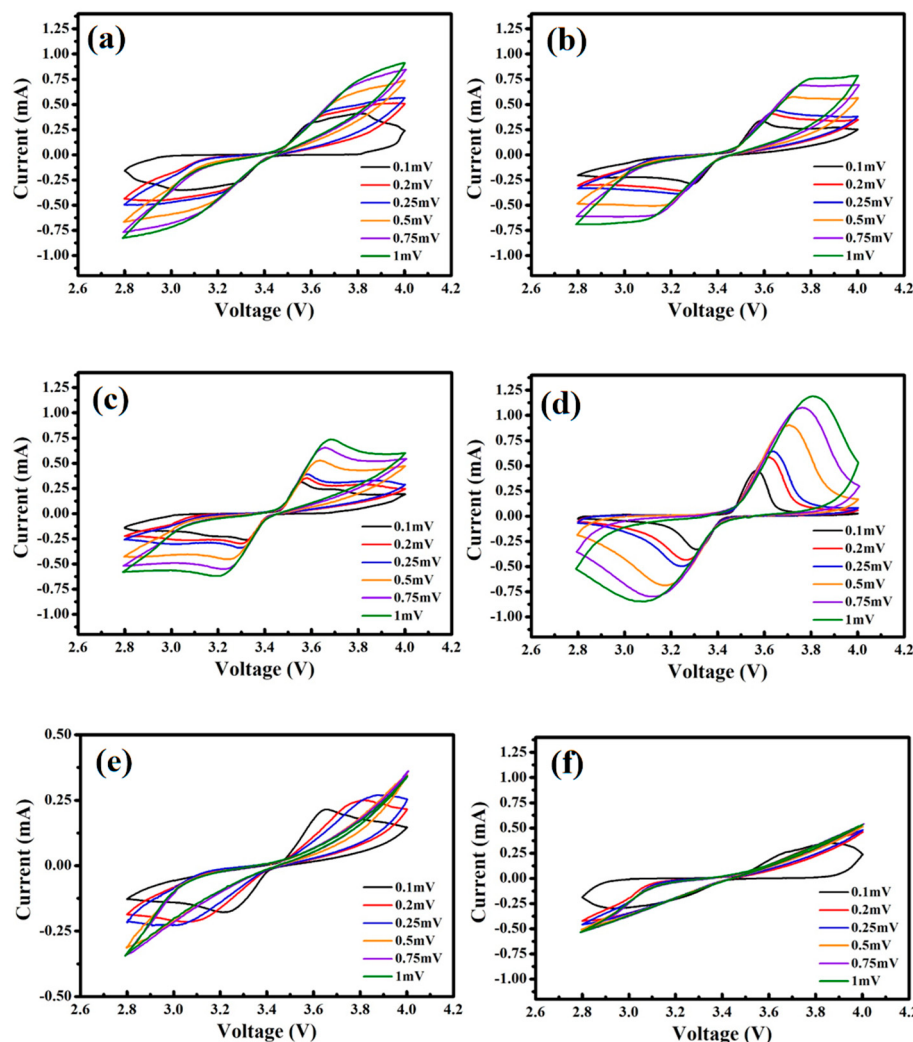


Figure 6. Cyclic voltammetry patterns of (a) SP_3%, (b) SP_4%, (c) SP_5%, (d) SP_5.5%, (e) SP_6%, and (f) SP_7% samples with different scanning rates of 0.1 to 1 mVs^{-1} between 2.8 and 4.0 V.

Table 4. The voltage difference (ΔV) of SP_3%, SP_4%, SP_5%, SP_5.5%, SP_6%, and SP_7% samples.

Sample	ΔV^*					
	0.1	0.2	0.25	0.5	0.75	1.0
SP_3%	0.77	---	---	---	---	---
SP_4%	0.30	0.39	0.42	0.60	1.00	---
SP_5%	0.26	0.35	0.39	0.54	0.64	0.73
SP_5.5%	0.23	0.28	0.29	0.39	0.43	0.49
SP_6%	0.44	0.75	0.92	---	---	---
SP_7%	0.91	---	---	---	---	---

* The ΔV is the voltage gap between maximum oxidation peak and minimum reduction peak and their voltage difference.

The peak current (I_p) was plotted as a function of the square root of the scan rate ($v^{1/2}$)—see Figure 7a–d. After linear fitting, a slope ($dI/dv^{1/2}$) can be obtained, which is substituted into the Randles–Sevcik Equation (Equation (3)) [49], and the D_{CV} value of the diffusion coefficient for the Li^+ ions in the battery can be calculated:

$$I_p = 0.4463CS \times [(nF)^{3/2}(D_{CV}v)^{1/2}/(RT)^{1/2}] \quad (3)$$

where D_{CV} : Li⁺ ion diffusion coefficient ($\text{cm}^2 \text{s}^{-1}$), I_p : peak indicated current (A), C: lithium ion concentration in the electrode (mole), S: pole piece area (cm^2), n: number of electrons transferred (mol), F: Faraday's constant ($96,500 \text{ C} \cdot \text{mol}^{-1}$), v: scan rate (V), R: gas constant ($8.314 \text{ J K}^{-1} \text{ mol}^{-1}$), and T: working temperature (K).

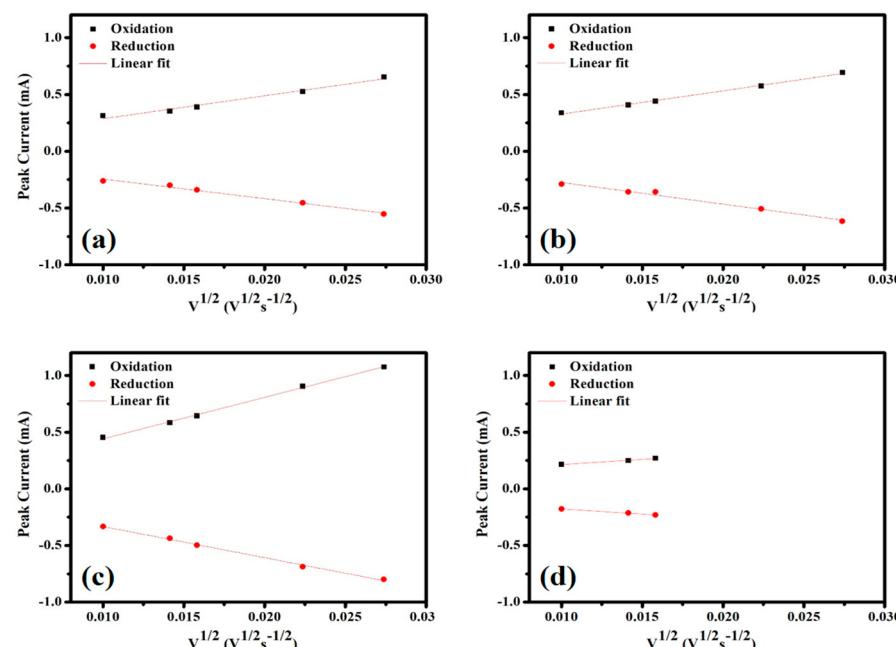


Figure 7. The relationships between peak current and scanning rate for (a) SP_4%, (b) SP_5%, (c) SP_5.5%, and (d) SP_6% samples.

Table 5 shows the calculated diffusion coefficients for the Li⁺ ions. According to the results, the maximum diffusion coefficient ($2.6 \times 10^{-10} \text{ cm}^2 \text{s}^{-1}$) of the Li⁺ ion was observed for SP_5.5%, and when the carbon content and the conductivity increased, the diffusion coefficient increased before it decreased.

Table 5. The diffusion coefficient D_{CV} of SP_4%, SP_5%, SP_5.5%, and SP_6% samples.

Sample	$D_{CV} (\text{cm}^2 \text{s}^{-1})$ Oxidation	$D_{CV} (\text{cm}^2 \text{s}^{-1})$ Reduction
SP_4%	7.95×10^{-11}	5.78×10^{-11}
SP_5%	8.18×10^{-11}	7.09×10^{-11}
SP_5.5%	2.60×10^{-10}	1.14×10^{-10}
SP_6%	1.63×10^{-11}	1.57×10^{-11}

Lithium served as the negative electrode in the battery, while LiFePO₄ with different quantities of conductive carbon was used as the positive electrode, with 1 M LiPF₆ and EC/EMC/DMC = 1:1:1 + 1 vol% VC as the electrolyte. The battery was placed in the Jiayou Technology BAT-750B charge/discharge apparatus and subjected to four distinct charge/discharge rates—0.1 C (600 min), 0.5 C (120 min), 1 C (60 min), 5 C (12 min), and 10 C (6 min)—at room temperature. Each sample had a cut-off voltage range of 2.8–4.0 V. The charge/discharge curves for the samples SP_3%, SP_4%, SP_5%, SP_5.5%, SP_6%, and SP_7% are shown in Figure 8a, with a charge/discharge rate of 0.1 C. The discharge capacities of SP_3%, SP_4%, SP_5%, SP_5.5%, SP_6%, and SP_7% were 135.1 mAh g⁻¹, 152.2 mAh g⁻¹, 152.9 mAh g⁻¹, 169.8 mAh g⁻¹, 139.2 mAh g⁻¹, and 129.2 mAh g⁻¹, respectively. SP_5.5% had the highest discharge capacity as well as the highest charge/discharge window. The intercalation and deintercalation of Li⁺ ions during the charge/discharge process are the basis of the charge/discharge platform. In other words,

this ratio improves Li^+ diffusion during the charge/discharge process and increases the discharge capacity.

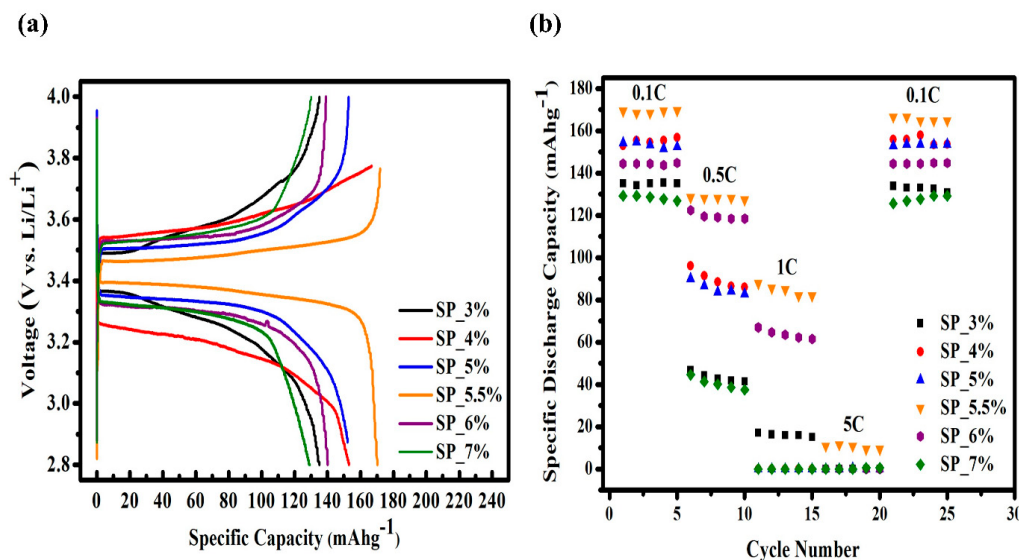


Figure 8. Electrochemical performance of SP_3%, SP_4%, SP_5%, SP_5.5%, SP_6%, and SP_7% samples between 2.8 and 4.0 V. (a) Initial charge/discharge curve at 0.1 C and (b) rate capacity at different current densities.

Furthermore, as the conductive carbon content increases, the sample's discharge capacity increases, peaking at 6% carbon. Subsequently, the capacity starts to decline due to insufficient binder presence. Taking into account the adhesion test results, this behavior is likely due to a weak bond between the particles and the Al substrate. Figure 8b displays the charge/discharge curves of each sample at different charge/discharge rates. The rates range from low to high, and the discharge capacity of every sample shows different degrees of decline. Notably, only SP_5.5% can successfully manage a 5 C high-rate charge/discharge. After four different charge/discharge rate tests and returning to 0.1 C, the discharge capacity was 166.5 mAh g^{-1} with a retention of 98%. These numbers indicate that, for this ratio, the structure did not collapse even following a high-rate charge/discharge, and the battery remained stable.

3. Materials and Methods

In this work, the positive electrode sample was prepared using LiFePO_4 , Super P (99%, Taiwan Libo, Taichung City, Taiwan), and poly (vinylidene fluoride), PVDF, (99%, Jingming Chemical, Taipei, Taiwan), which were mixed in the solvent N-methyl pyrrolidone, NMP, (99%, Jingming Chemical) with different weight ratios. The amount of Super P varied (3%, 4%, 5%, 5.5%, 6%, and 7%) to study the effect on the electrochemical properties. The sample ratios used are shown in Table 6. Firstly, PVDF was added to NMP, centrifuged, and left for 1 h so that the powder dissolved completely. Then, LiFePO_4 powder was added with different amounts of Super P, centrifuged, and left again for 1 h to form a slurry after mixing. The slurry was evenly applied to the aluminum foil using the doctor blade method with a $200 \mu\text{m}$ squeegee. The sample was then subjected to a vacuum at 100°C for 48 h to remove residual solvent, resulting in the preparation of the LiFePO_4 cathode sheet. In addition to the Super P content, the coating thickness is very important to improve the homogeneity of the Li-ion flux. Therefore, we controlled the coating thickness by adjusting the viscosity of the slurry and the withdrawal speed during the doctor blade coating process. Specifically, we prepared slurries with different viscosities by varying the NMP solvent content and adjusting the coating speed to obtain the desired coating thickness. We also used a micrometer to measure the thickness to ensure consistency and accuracy. Furthermore, the sheet was rolled and cut into small discs with a diameter of

13 mm to complete the production of the positive electrode. The vacuum-dried cathode piece was then cut into a small disc with a diameter of 13 mm for use in a standard R2032 coin cell. The coin cells were assembled inside a glove box in an argon atmosphere with lithium as the anode and $1 \text{ mol LiPF}_6 + \text{EC/EMC/DMC} = 1:1:1 \text{ vol\%} + 1\% \text{ VC}$ electrolyte, while keeping a standardized electrolyte-to-electrode ratio of $5 \mu\text{L}/\text{mg}$. After keeping the sample in the same atmosphere for one day, the electrochemical performance test was carried out. The gravimetric loading of the LFP cathodes was 24.18 mg/cm^2 and the 1C current density was 0.54604 mA/cm^2 .

Table 6. Ratio of the sample components for positive electrode preparation.

Sample Name	LiFePO ₄ (wt%)	Super P (wt%)	PVDF (wt%)
SP_3%	88	3	9
SP_4%	88	4	8
SP_5%	88	5	7
SP_5.5%	88	5.5	6.5
SP_6%	88	6	6
SP_7%	88	7	5

An electrochemical analysis and examination of the properties of the prepared cathodes were performed as follows: The particle size and morphology of the Super P conductive carbon material powder were observed using field emission scanning electron microscopy (FE-SEM, JEOL JSM-6701F, Tokyo, Japan). A laser particle size analyzer (Beckman Coulter Particle Analyzer PN A54412, Brea, CA, USA) was used for the dynamic light scattering (DLS) analysis. An adhesion tester (MIT-AT12, Taichung City, Taiwan) was used to evaluate the positive LiFePO₄ electrodes made of different amounts of conductive carbon. For the adhesive force measurement, after cutting the grid pattern and penetrating the coating, it was pasted with a special test tape according to the peeling of the coating. The adhesion of the coating to the substrate separation was evaluated and classified into six grades to assess its quality. Cyclic voltammetry (CV) was performed using a potentiostat (Jihah-5640, Taipei, Taiwan) at different scan rates ($0.1, 0.2, 0.25, 0.5, 0.75$, and 1 mVs^{-1}) with a voltage range of $2.8\text{--}4.0 \text{ V}$. Electrochemical impedance spectroscopy (EIS) was performed using a potentiostat (VSP-300, BioLogic, Seyssinet-Pariset, France) at $0.01\text{--}7 \text{ MHz}$ under open circuit voltage. The capacity and rate performance of the fabricated coin cells were evaluated using a charge/discharge cell test instrument (Acutech Systems, BAT-750B, New Taipei City, Taiwan).

4. Conclusions

The explanations above and our experimental results present some compelling conclusions. This study used alternative conductive carbon materials (Super P) as the active material content to enhance the conductivity and compatibility of the cathode in lithium-ion batteries. The adhesion test indicates that when the amount of Super P increased to 5.5%, the ASTM grade could still reach 3B. However, when it increased beyond 6% or 7%, adhesion started to decrease significantly, which affected the electrochemical performance. Similarly, as the amount of conductive carbon material increased (and the amount of binder decreased), the adhesion gradually decreased. Moreover, the analysis of the cyclic voltammetry data revealed that within the range of 3% to 5.5% Super P content, a reduction in polarization in LiFePO₄ occurred. This reduction impacted the diffusion coefficient of Li⁺ ions positively, enhancing their mobility within the material. However, when the Super P content exceeded this range, the adhesion between particles decreased, which resulted in the closure of diffusion paths for Li⁺ ions. This led to increased polarization and a reduced overall performance. The charge/discharge test determined that the initial discharge capacity of the SP_5.5% sample (at a charge/discharge rate of 0.1 C) was as high as 169.8 mAh g^{-1} . This number is very close to the theoretical capacity of LiFePO₄ (170 mAh g^{-1}), and only the SP_5.5% sample could manage a high-rate charge/discharge of 5 C. The EIS AC

impedance analysis suggests that SP_5.5% has the lowest charge-transfer impedance (67Ω) and the highest Li^+ ion diffusion coefficient ($5.76 \times 10^{-14} \text{ cm}^2 \text{ s}^{-1}$). Clearly, conductive carbon helped improve the conductivity, but adding too much led to insufficient connectivity between the conductive carbon particles, which reduced conductivity. As a result, the optimal ratio of the three ingredients was determined as follows: LiFePO_4 at 88%, Super P at 5.5%, and PVDF at 6.5%. This balanced composition promotes the efficient diffusion of Li^+ ions during the charge/discharge process. In addition, it contributes to improved performance, particularly in high-rate charging and discharging scenarios.

Author Contributions: D.M. conceptualization, methodology, investigation, data curation, writing—original draft preparation; M.-J.C., investigation, data curation, formal analysis; I.-M.H., conceptualization, supervision, funding acquisition, writing—review and editing. All authors have read and agreed to the published version of the manuscript.

Funding: Financial support for this work was provided by the National Science and Technology Council in Taiwan through grant number MOST 110-2622-E-155-011.

Data Availability Statement: The data that support the findings of this study are available from the corresponding author upon reasonable request.

Conflicts of Interest: The authors declare no conflict of interest.

References

- Deng, D. Li-ion batteries: Basics, progress, and challenges. *Energy Sci. Eng.* **2015**, *3*, 385–418. [[CrossRef](#)]
- Yang, K.; Liu, Z.; Chai, J.; Zheng, Y.; Fu, X.; Shen, Y.H.; Chen, J.; Liu, Z.; Shi, S. High performance polyimide-based separator for 4.5 V high voltage LiCoO_2 battery with superior safety. *Mater. Chem. Phys.* **2022**, *282*, 125975–125983. [[CrossRef](#)]
- Mohanty, D.; Huang, P.H.; Hung, I.M. Preparation and Characterization of a LiFePO_4 -Lithium Salt Composite Cathode for All-Solid-State Li-Metal Batteries. *Batteries* **2023**, *9*, 236. [[CrossRef](#)]
- Guo, J.; Zhang, J.; Chen, C.; Lan, Y. Rapid photodegradation of methyl orange by oxalic acids assisted with cathode material of lithium ion batteries LiFePO_4 . *J. Taiwan Inst. Chem. Eng.* **2016**, *62*, 187–191. [[CrossRef](#)]
- Geng, J.; Zou, Z.; Wang, T.; Zhang, S.; Ling, W.; Peng, X.; Liang, F. Synthesis and modification mechanism of vanadium oxide coated LiFePO_4 cathode materials with excellent electrochemical performance. *Nanotechnology* **2023**, *34*, 445403–445412. [[CrossRef](#)]
- Yang, C.C.; Jang, J.H.; Jiang, J.R. Preparation of carbon and oxide co-modified LiFePO_4 cathode material for high performance lithium-ion battery. *Mater. Chem. Phys.* **2015**, *165*, 196–206. [[CrossRef](#)]
- Kraytsberg, A.; Ein-Eli, Y. Higher, Stronger, Better... A Review of 5 Volt Cathode Materials for Advanced Lithium-Ion Batteries. *Adv. Energy Mater.* **2012**, *2*, 922–939. [[CrossRef](#)]
- Liu, H.; Liu, Y.; An, L.; Zhao, X.; Wang, L.; Liang, G. High Energy Density LiFePO_4/C Cathode Material Synthesized by Wet Ball Milling Combined with Spray Drying Method. *J. Electrochem. Soc.* **2017**, *164*, A3666–A3672. [[CrossRef](#)]
- Nie, Z.; Liu, Y.; Yang, L.; Li, S.; Pan, F. Construction and Application of Materials Knowledge Graph Based on Author Disambiguation: Revisiting the Evolution of LiFePO_4 . *Adv. Energy Mater.* **2021**, *11*, 2003580–2003584. [[CrossRef](#)]
- Cramer, C.L.; Lonescu, E.; Zajac, M.G.; Nelson, A.T.; Katoh, Y.; Haslam, J.J.; Wondraczek, L.; Aguirre, T.G.; LeBlanc, S.; Wang, H.; et al. Additive manufacturing of ceramic materials for energy applications: Road map and opportunities. *J. Eur. Ceram. Soc.* **2022**, *42*, 3049–3088. [[CrossRef](#)]
- Zhang, F.; Qi, L. Recent Progress in Self-Supported Metal Oxide Nanoarray Electrodes for Advanced Lithium-Ion Batteries. *Adv. Sci.* **2016**, *3*, 1600049–1600077. [[CrossRef](#)]
- Tang, X.C.; Li, L.X.; Lai, Q.L.; Song, X.W.; Jiang, L.H. Investigation on diffusion behavior of Li^+ in LiFePO_4 by capacity intermittent titration technique (CITT). *Electrochim. Acta* **2009**, *54*, 2329–2334. [[CrossRef](#)]
- Gao, C.; Zhou, J.; Liu, G.; Wang, L. Lithium-ions diffusion kinetic in LiFePO_4 /carbon nanoparticles synthesized by microwave plasma chemical vapor deposition for lithium-ion batteries. *App. Surf. Sci.* **2018**, *433*, 35–44. [[CrossRef](#)]
- Li, J.; Yuan, C.F.; Guo, Z.H.; Zhang, Z.A.; Lai, Y.Q.; Liu, J. Limiting factors for low-temperature performance of electrolytes in $\text{LiFePO}_4/\text{Li}$ and graphite/Li half cells. *Electrochim. Acta* **2012**, *59*, 69–74. [[CrossRef](#)]
- Zhang, S.S.; Jow, T.R. Aluminum corrosion in electrolyte of Li-ion battery. *J. Power Sources* **2002**, *109*, 458–464. [[CrossRef](#)]
- Zhang, S.S.; Xu, K.; Jow, T.R. The low temperature performance of Li-ion batteries. *J. Power Sources* **2003**, *115*, 137–140. [[CrossRef](#)]
- Zhang, S.S.; Xu, K.; Jow, T.R. Electrochemical impedance study on the low temperature of Li-ion batteries. *Electrochim. Acta* **2004**, *49*, 1057–1061. [[CrossRef](#)]
- Chang, W.; Kim, S.J.; Park, I.T.; Cho, B.W.; Chung, K.Y.; Shin, H.C. Low temperature performance of LiFePO_4 cathode material for Li-ion batteries. *J. Alloys Compd.* **2013**, *563*, 249–253. [[CrossRef](#)]

19. Shu, H.; Chen, M.; Fu, Y.; Yang, X.; Yi, X.; Bai, Y.; Liang, Q.; Wei, Q.; Hu, B.; Tan, J.; et al. Improvement of electrochemical performance for spherical LiFePO₄ via hybrid coated with electron conductive carbon and fast Li ion conductive La_{0.56}Li_{0.33}TiO₃. *J. Power Sources* **2014**, *252*, 73–78. [CrossRef]
20. Wang, K.X.; Li, X.H.; Chen, J.S. Surface and Interface Engineering of Electrode Materials for Lithium-Ion Batteries. *Adv. Mater.* **2015**, *27*, 527–545. [CrossRef]
21. Sangeeta; Agnihotri, S.; Arya, A.; Sharma, A.L. Improved electrochemical performance of the Cr doped cathode materials for energy storage/conversion devices. *AIP Conf. Proc.* **2016**, *1728*, 020380. [CrossRef]
22. Yao, J.; Wu, F.; Qiu, X.; Li, N.; Su, Y. Effect of CeO₂-coating on the electrochemical performances of LiFePO₄/C cathode material. *Electrochim. Acta* **2011**, *56*, 5587–5592. [CrossRef]
23. Weiss, M.; Ruess, R.; Kasnatchew, J.; Levartovsky, Y.; Lexy, N.R.; Minnmann, P.; Stolz, L.; Waldmann, T.; Mehren, M.; Aurbach, D.; et al. Fast Charging of Lithium-Ion Batteries: A Review of Materials Aspects. *Adv. Energy Mater.* **2021**, *11*, 2101126–2101162. [CrossRef]
24. Weng, J.; Peng, L. Improving the electrochemical performance of LiFePO₄ cathode with novel water-soluble binders. *Mater. Chem. Phys.* **2022**, *290*, 126530–126534. [CrossRef]
25. Örnek, A.; Bulut, E.; Özcar, M. The chemical, physical and electrochemical effects of carbon sources on the nano-scale LiFePO₄ cathode surface. *Ceram. Int.* **2014**, *40*, 15727–15736. [CrossRef]
26. Miao, C.; Bai, P.; Jiang, Q.; Sun, S.; Wang, X. A novel synthesis and characterization of LiFePO₄ and LiFePO₄/C as a cathode material for lithium-ion battery. *J. Power Sources* **2014**, *246*, 232–238. [CrossRef]
27. Lin, Y.; Gao, M.X.; Zhu, D.; Liu, Y.F.; Pan, H.G. Effects of carbon coating and iron phosphides on the electrochemical properties of LiFePO₄/C. *J. Power Sources* **2008**, *184*, 444–448. [CrossRef]
28. Al-Salih, H.; Houache, M.S.E.; Baranova, E.A.; Abu-Lebdeh, Y. Composite Cathodes for Solid-State Lithium Batteries: “Catholytes” the Underrated Giants. *Adv. Energy Sustain. Res.* **2022**, *3*, 2200032–2200046. [CrossRef]
29. Nguyen, V.A.; Kuss, C. Review—Conducting Polymer-Based Binders for Lithium-Ion Batteries and Beyond. *J. Electrochem. Soc.* **2020**, *167*, 065501–065516. [CrossRef]
30. Wei, M.; Zhang, F.; Wang, W.; Alexandridis, P.; Zhou, C.; Wu, G. 3D direct writing fabrication of electrodes for electrochemical storage devices. *J. Power Sources* **2017**, *354*, 134–147. [CrossRef]
31. Zhao, N.; Li, Y.; Zhao, X.; Zhi, X.; Liang, G. Effect of particle size and purity on the low temperature electrochemical performance of LiFePO₄/C cathode material. *J. Alloys Compd.* **2016**, *683*, 123–132. [CrossRef]
32. Cheng, F.; Wan, W.; Tan, Z.; Huang, Y.; Zhou, H.; Chen, J.; Zhang, X. High power performance of nano-LiFePO₄/C cathode material synthesized via lauric acid-assisted solid-state reaction. *Electrochim. Acta* **2011**, *56*, 2999–3005. [CrossRef]
33. Yang, C.C.; Hung, Y.W.; Lue, S.J. The Carbon Additive Effect on Electrochemical Performance of LiFe_{0.5}Mn_{0.5}PO₄/C Composites by a Simple Solid-State Method for Lithium Ion Batteries. *Batteries* **2016**, *2*, 18. [CrossRef]
34. Liu, H.; Miao, C.; Meng, Y.; He, Y.B.; Xu, Q.; Zhang, X.; Tang, Z. Optimized synthesis of nano-sized LiFePO₄/C particles with excellent rate capability for lithium ion batteries. *Electrochim. Acta* **2014**, *130*, 322–328. [CrossRef]
35. Eftekhari, A. LiFePO₄/C nanocomposites for lithium-ion batteries. *J. Power Sources* **2017**, *343*, 395–411. [CrossRef]
36. Zhang, B.; Xu, Y.; Wang, J.; Lin, J.; Wang, C.; Chen, Y. Lanthanum and cerium Co-doped LiFePO₄: Morphology, electrochemical performance and kinetic study from –30–+50 °C. *Electrochim. Acta* **2019**, *322*, 134686–134695. [CrossRef]
37. Yang, W.; Bi, Y.; Qin, Y.; Liu, Y.; Zhang, X.; Yang, B.; Wu, Q.; Wang, D.; Shi, S. LiMn_{0.8}Fe_{0.2}PO₄/C cathode material synthesized via co-precipitation method with superior high-rate and low-temperature performances for lithium-ion batteries. *J. Power Sources* **2015**, *275*, 785–791. [CrossRef]
38. Lin, Y.; Lin, Y.; Zhou, T.; Zhao, G.; Huang, Y.; Huang, Z. Enhanced electrochemical performances of LiFePO₄/C by surface modification with Sn nanoparticles. *J. Power Sources* **2013**, *226*, 20–26. [CrossRef]
39. Jiang, Q.; Zhang, H.; Ren, Z.; Ma, H.; Xue, M. Recent progresses of metal-organic framework-based materials in electrochemical energy storage. *Mater. Today Sustain.* **2022**, *19*, 100174–100205. [CrossRef]
40. Li, X.; Sun, X.; Hu, X.; Fan, F.; Cai, S.; Zheng, C.; Stucky, G.D. Review on comprehending and enhancing the initial Coulombic efficiency of anode materials in lithium-ion/sodium-ion batteries. *Nano Energy* **2020**, *77*, 105143–105162. [CrossRef]
41. Mauger, A.; Julien, C.; Paolella, A.; Armand, M.; Zaghib, K. Recent Progress on Organic Electrodes Materials for Rechargeable Batteries and Supercapacitors. *Materials* **2019**, *12*, 1770. [CrossRef] [PubMed]
42. Song, M.K.; Park, S.; Alamgir, F.M.; Cho, J.; Liu, M. Nanostructured electrodes for lithium-ion and lithium-air batteries: The latest developments, challenges, and perspectives. *Mater. Sci. Eng. R Rep.* **2011**, *72*, 203–252. [CrossRef]
43. Ellis, B.L.; Lee, K.T.; Nazar, L.F. Positive Electrode Materials for Li-Ion and Li-Batteries. *Chem. Mater.* **2010**, *22*, 691–714. [CrossRef]
44. Yousaf, M.; Shi, H.T.H.; Wang, Y.; Chen, Y.; Ma, Z.; Cao, A.; Naguib, H.A.; Han, R.P.S. Novel Pliable Electrodes for Flexible Electrochemical Energy Storage Devices: Recent Progress and Challenges. *Adv. Energy Mater.* **2016**, *6*, 1600490–1600512. [CrossRef]
45. Zhang, Y.; Liu, Z.; Wang, Z.; Jiang, Y.; Wen, G.; Gao, P.; Zhu, Y. Electrochemical impedance spectroscopy study of lithium-rich material 0.5Li₂MnO₃·0.5LiNi_{1/3}Co_{1/3}Mn_{1/3}O₂ in the first two charge-discharge cycles. *Electrochim. Acta* **2019**, *310*, 136–145. [CrossRef]
46. Mohanty, D.; Chen, S.Y.; Hung, I.M. Effect of Lithium Salt Concentration on Materials Characteristics and Electrochemical Performance of Hybrid Inorganic/Polymer Solid Electrolyte for Solid-State Lithium-Ion Batteries. *Batteries* **2022**, *8*, 173. [CrossRef]

47. Mohanty, D.; Lu, Z.L.; Hung, I.M. Effect of carbon coating on electrochemical properties of $\text{Li}_3\text{V}_2(\text{PO}_4)_3$ cathode synthesized by citric-acid gel method for lithium-ion batteries. *J. Appl. Electrochem.* **2023**, *53*, 1003–1013. [[CrossRef](#)]
48. Rudy, A.; Mironenko, A.; Naumov, V.; Novozhilova, A.; Skundin, A.; Fedorov, I. Determination of Diffusion Coefficients of Lithium in Solid Electrolyte LiPON. *Batteries* **2021**, *7*, 21. [[CrossRef](#)]
49. Ngamchuea, K.; Eloul, S.; Tschulik, K.; Compton, R.G. Planar diffusion to macro disc electrodes—What electrode size is required for the Cottrell and Randles-Sevcik equations to apply quantitatively? *J. Solid State Electrochem.* **2014**, *18*, 3251–3257. [[CrossRef](#)]

Disclaimer/Publisher’s Note: The statements, opinions and data contained in all publications are solely those of the individual author(s) and contributor(s) and not of MDPI and/or the editor(s). MDPI and/or the editor(s) disclaim responsibility for any injury to people or property resulting from any ideas, methods, instructions or products referred to in the content.